

Received 4 July 2025, accepted 20 July 2025, date of publication 30 July 2025, date of current version 5 August 2025.

Digital Object Identifier 10.1109/ACCESS.2025.3593957



Indoor Human Motion Recognition Based on FMCW Radar and Threshold **Comparison Algorithm**

RUOYU HE¹⁰, MASAKI KUROSAWA¹⁰, AND GUANGHAO SUN¹⁰, (Senior Member, IEEE) Graduate School of Informatics and Engineering, The University of Electro-Communications, Tokyo 182-8585, Japan

Corresponding author: Guanghao Sun (Guanghao.Sun@uec.ac.jp)

This work involved human subjects or animals in its research. Approval of all ethical and experimental procedures and protocols was granted by the Committee on Human Research of the University of Electro-Communications.

ABSTRACT Radar technology, particularly frequency-modulated continuous wave (FMCW) radar, has garnered attention in the field of smart home monitoring owing to its high sensitivity, long-range surveillance capabilities, and privacy-preserving characteristics. This study proposed a human motion state recognition system to recognize motion states based on the spectra from radar signals in a home environment. The velocity of a target is assessed by comparing a micro-Doppler signature against a velocity threshold, and its height signature discerns between high and low postures against a height threshold. The horizontal position of the target is determined using a range-angle map. The proposed threshold algorithm defines the motion state using the velocity, height postures and indoor position. Subsequently, the performance of the system is evaluated by conducting experiments on 10 subjects. The results demonstrate the efficacy of the proposed method, achieving an accuracy of approximately 85%. In continuous-action experiments involving sequences of movements, the system achieved recognition accuracy exceeding 90%.

INDEX TERMS FMCW radar, threshold comparing, smart home, motion recognition.

I. INTRODUCTION

In recent years, many countries have witnessed a rapid increase in their aging populations, coupled with a growing concern for the well-being of disabled individuals. Consequently, there is an increasing demand for indoor single-room vital sign monitoring in both households and facilities. Thus, monitoring movement is imperative for individuals with limited mobility [1].

Previous studies have often relied on cameras or thermal imagers to monitor indoor movement status. However, cameras are heavily dependent on ambient light conditions [2], making them less effective at night, when monitoring is crucial. However, thermal imagers are highly sensitive to indoor temperatures, which makes them susceptible to variations caused by diurnal or seasonal changes. Moreover, cameras pose significant privacy concerns, and even with blurred

The associate editor coordinating the review of this manuscript and approving it for publication was Eunkyoung Park.

images to address this issue, the quality of research data is compromised [3].

Radar sensors provide significant benefits in home healthcare. Radar sensors emit radio waves and detect their reflections, which enables the noncontact monitoring of individuals [4] while ensuring privacy and eliminating the need for physical contact or visual exposure. Additionally, radar sensors are less affected by environmental factors, such as lighting variations or physical obstructions, which makes them suitable for monitoring in various home environments. Moreover, radar sensors can penetrate certain materials, thus enabling monitoring through walls or furniture and further enhancing their versatility in home healthcare applications [5], [6]. Furthermore, radar sensors can capture motion and vital signs with high accuracy, thereby allowing for the continuous and real-time monitoring of activities, respiration, heart rate, and sleep patterns [7], [8], [9].

Frequency-modulated continuous-wave (FMCW) radar is an advanced technology that is gaining attention in home



healthcare. An FMCW radar operates by continuously transmitting a signal with a frequency that changes over time. An FMCW radar measures the frequency shift of a returned signal to determine the range, velocity, and other features of an object or individual within its range [10]. This technology offers several advantages for home healthcare applications, including noncontact monitoring, the ability to penetrate obstacles, and high accuracy in detecting movements and vital signs [11].

II. RELATED WORKS

A. EXISTING WORKS

This section highlights the advantages of our proposed method over existing methods by presenting an overview of the comparison between the proposed method and existing methods, focusing on indoor target motion state recognition via Doppler radar.

Recognition methods commonly found in the literature typically analyze radar data as snapshots captured within a finite time window and focus on a single activity or gait without considering continuous, long-term motion, which is particularly important for in-home monitoring. Moreover, motion states are often constrained in a predetermined direction that is aligned with the line of sight of the radar. Existing classification algorithms encompass traditional classifiers [12], such as support vector machines (SVMs), K-nearest neighbors (KNNs), random forests [5], and decision trees. Alternative approaches include autoencoders (AEs) [13], convolutional neural networks (CNNs) [14], [15], and recurrent neural networks (RNNs), particularly long short-term memories (LSTMs) [16], [17] and superimposed gated recurrent units (SGRUs) [18].

Shamsfakhr used an FMCW radar platform to collect data on human localization and walking trajectories as well as performed target identification and tracking for long-term motions using a combined trajectory-oriented multi-hypothesis tracking (TOMHT) + extended Kalman filter approach and an expectation maximization (EM)-based approach, respectively [19]. Rana et al. used a ultrawideband (UWB) radar as a non-invasive biosensor that was designed to be applied in real home environments and connected via an Internet of Things (IoT) platform. This system brought greater intelligence and understanding to recognize the condition of a person over time and could remotely access control when needed [20], [21].

The common, existing methods used in these studies mainly involve machine learning algorithms and neural networks for classification. Machine learning-based approaches have shown high accuracy in human motion recognition tasks, but they generally require high computational resources and extensive training data [22]. On the other hand, although the combination of feature extraction and SVM can achieve higher classification accuracy and can be implemented in real time on low-cost embedded processing devices, it still requires a certain amount of training

resources, and the analysis of generalization ability is not rigorous enough [23]. There are also detection algorithms that do not use machine-learning algorithms and instead use threshold comparators. This method uses a detector based on the standard deviation estimation of the peak amplitude differences and a threshold comparator to distinguish small body movements and perform breath detection [24]. Yoo proposed a non-learning, three-stage sleep-detection algorithm using a 61 GHz FMCW radar sensor. The breathing and motion information characteristics of each sleep stage were extracted from the radar signals acquired by the subject during the sleep state and used as a characterization factor against the study target for non-learning-based, three-stage sleep detection using estimated thresholds and biometric information [9]. Zhao and Xue detected human signals using a UWB radar that automatically identified the location of human and mechanical vibrations using a constant false alarm rate algorithm. New features are then extracted by calculating the half-height width of the target wavelet entropy to distinguish between humans and animals as well as humans and moving objects [25], [26].

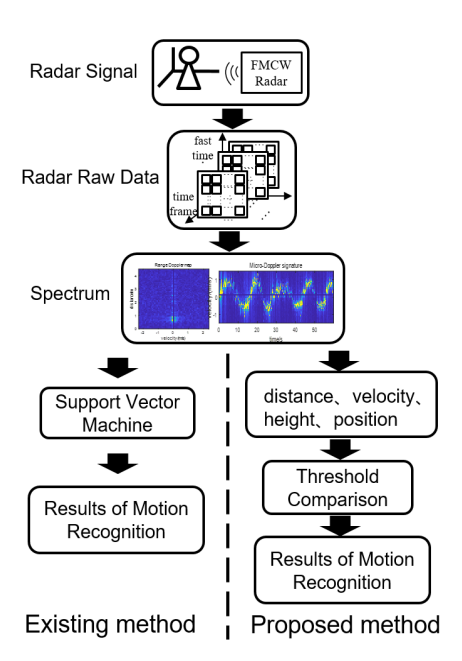


FIGURE 1. Comparison of the existing and proposed methods. This figure illustrates the overall workflow of conventional machine learning-based methods versus the proposed threshold comparison method. It highlights the differences in data processing, including the input of RD maps and micro-Doppler signatures, and emphasizes the reduced complexity and improved efficiency of our approach.

B. COMPARISON WITH EXISTING WORKS

In Fig. 1, existing methods primarily involve feeding the RDmap or Doppler spectrum obtained from the radar into neural networks or SVM to derive classification models for motion recognition. However, although achieving higher accuracy, typically involve significantly greater computational overhead and resource consumption, which restricts



FIGURE 2. Motion monitoring system overview. The diagram presents the complete system architecture for indoor motion monitoring using FMCW radar. It details the flow from raw radar signal acquisition, through feature extraction (velocity, height, and position), to the final threshold-based motion classification, with annotations on key processing steps and threshold criteria.

their practical deployment in real-time edge computing scenarios. Recent threshold-based methodologies, primarily utilized micro-Doppler features for motion recognition. Despite their low computational load, these methods have limitations in robustness when dealing with varied human motions or environmental disturbances.

Considering practical indoor environments characterized by diverse room layouts, varying physical characteristics of monitored subjects, and constraints related to energy consumption and processing time, this study proposes a method for indoor target motion state monitoring using an FMCW radar based on the threshold comparison shown in Fig. 2. Moreover, this study compares the proposed method with existing machine learning techniques.

1) REDUCED COMPLEXITY

No training datasets, models, or procedures are required, which leads to a simplified implementation process that is expected to be implemented in smaller processing units.

2) LOWER RESOURCE REQUIREMENTS

The method proposed in this study eliminates the need for large amounts of labeled data for training, thereby reducing data collection. This is particularly advantageous in scenarios in which annotated data are scarce or expensive to acquire.

3) INCREASED ROBUSTNESS

By relying on direct feature extraction from the RDmap and RAmap, the proposed method was found to be less susceptible to noise, variations in environmental conditions, and target features. This robustness ensures reliable motion state monitoring, even in challenging indoor environments.

III. PRINCIPLE

Frequency-modulated continuous-wave (FMCW) radar is a type of radar system commonly used for distance, velocity,

and motion state recognition.

$$s_m(\tau) = cos\left(2\pi\left(f_0\tau + \frac{B}{2t_w}\tau^2\right)\right), \quad \tau \in [0, t_w]$$
 (1)

The radar transmits the number m (from 0 to M-1) transmitted wave $s_m(\tau)$ at time τ as described by (1). These transmissions occur at a time interval of t_p . Here, B is the frequency bandwidth, f_0 is the frequency, t_w is the width of the transmitted wave in one chirp, and T (> Mt_p) is the length of one time frame.

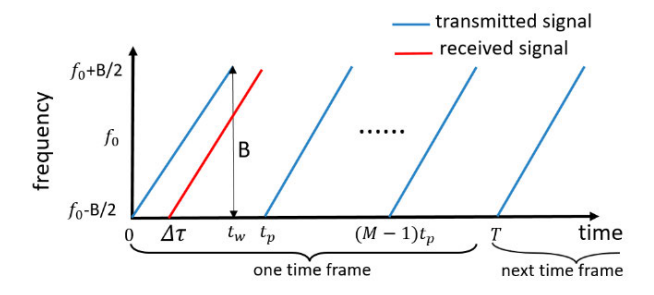


FIGURE 3. Signals of the transmitted and received signals in the frequency domain. This figure displays both the transmitted and received radar signals in the frequency domain. It demonstrates the frequency modulation process and the formation of beat signals, which are essential for determining target range and velocity.

When the chirp signal encounters an object, it reflects back to the radar system, and the received signal r_{mk} (τ) is represented by (2), where k is the antenna number and $\Delta \tau$ is the time difference between the received and transmitted signals. Figure 3 shows the transmitted signal s_m (τ) and received signal r_{mk} (τ) for a received antenna.

$$r_{mk}(\tau) = s_m(\tau - \Delta \tau) \tag{2}$$

Each received signal is sampled between 0 and t_w at an interval of τ_s . Therefore, the sampling timing becomes 0, $\tau_s, \dots, p\tau_s, \dots, (P-1)\tau_s$ $(p=0, \dots, P-1)$. The received signal is mixed with the transmitted signal, resulting in a beat



signal $b_{mk}(\tau)$ represented by (3).

$$b_{mk}(p\tau_s) = r_{mk}(p\tau_s) \times s_m(p\tau_s)^*$$
(3)

In Fig. 4, the range Doppler map, also known as an RD map, is a three-dimensional representation calculated from the received signals of an FMCW radar. The strength or intensity of each point is represented in a two-dimensional plane. The RDmap is calculated from the beat frequency signal through a 2-dimensional Fourier transform, as follows.

$$RD_k(d, v, nT) = FT_m \left\{ FT_p \left\{ b_{mk} \left(p\tau_s \right) \right\} \right\} \tag{4}$$

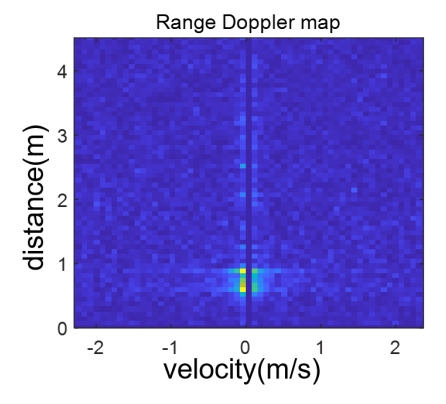


FIGURE 4. Range Doppler map. The range Doppler map shown here plots target velocity (x-axis) against range (y-axis) with signal intensity indicated by color gradations. It serves as the basis for extracting motion features necessary for state recognition.

Here, n represents the number of timeframes and k is the number of antennas from 0 to 2, where 0, 1, 0, and 2 are sets of horizontal or vertical antennas. Therefore, each timeframe can yield three RD maps: RD_0 , RD_1 and RD_2 . As shown in Fig. 5, Tx is the radar signal transmitting antenna, and Rx is the radar signal receiving antenna.

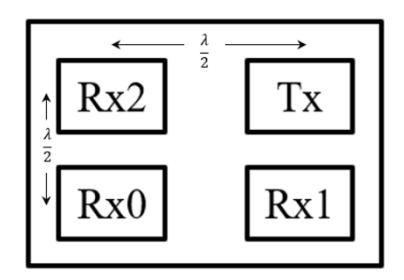


FIGURE 5. Radar antenna arrangement ($\lambda = \frac{c}{f_0}$: wavelength of radar transmitting wave). This figure depicts the physical layout of the radar's transmitting and receiving antennas. The arrangement facilitates accurate measurement of horizontal and vertical angles, which are critical for localizing targets within the monitored area.

Figure 6 shows that the RD maps obtained from the two receiving antennas in the same direction can be obtained by changing the phase and then overlaying it to obtain the signal strength at each assumed angle. Subsequently, the point with the highest strength was selected, whose corresponding angle was the angle at which the target was located. By deleting

points for other angles, a map of distance and angle relationships can be obtained. This map is called the range–angle map (Ramap). The calculation equations are as follows.

$$RA_{H}(d, \theta_{1}, nT) = \max_{v} \{ |RD_{0}(d, v, nT) + \exp(-j\frac{\sin\theta_{1}}{2})RD_{1}(d, v, nT) | \}$$

$$RA_{V}(d, \theta_{2}, nT) = \max_{v} \{ |RD_{0}(d, v, nT) + \exp(-j\frac{\sin\theta_{2}}{2})RD_{2}(d, v, nT) | \}$$

$$(6)$$

Here, θ_1 is the horizontal angle of arrival of the target, and θ_2 is the vertical angle of arrival of the target.

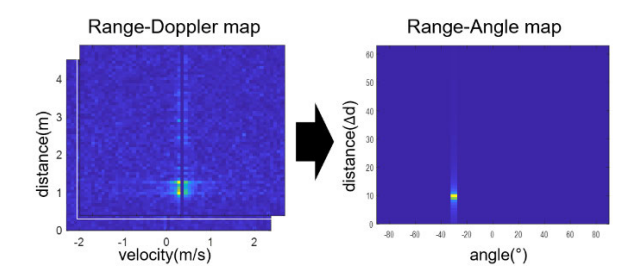


FIGURE 6. Range–Doppler map to range–angle map calculations. This diagram explains the process of transforming a range–Doppler map into a range–angle map. It details the phase adjustment and overlaying procedures used to pinpoint the target's angle of arrival, enhancing the precision of target positioning.

IV. METHODS AND PROCEDURES

A. RDmap EXTRACTION

RDmaps derived from the FMCW radar are valuable for target detection and analysis. However, the presence of noise and clutter in received signals can hinder accurate target identification. We proposed a target extraction method that utilizes RDmaps to enhance target detection by synthesizing a composite RDmap (cRDmap) and subsequently generating a μ RDmap that contains focused target information.

$$cRD(d, v, \theta_1, \theta_2, nT)$$

$$= RD_0(d, v, nT) + exp\left(-j\frac{sin\theta_1}{2}\right)RD_1(d, v, nT)$$

$$+ exp\left(-j\frac{sin\theta_2}{2}\right)RD_2(d, v, nT)$$
(7)

The next step involves extracting target information from cRDmap to create a μ RDmap. The extraction process focuses on selecting the range frames corresponding to the location of a target and a specific range window around it, as shown in (8):

$$\mu RD(d, v, \theta_1, \theta_2, nT) = cRD(d_l, v_h, \theta_1, \theta_2, nT)$$
 (8)

where:

$$d = d_l = d_0(n) + l \times \Delta d$$
, and $|l| < L \in \mathbb{Z}$,
 $v = v_h h \times \Delta v$, and $|h| < H \in \mathbb{Z}$

The μ RDmap is the area in the red box shown n Fig. 7, where d_l is the range within a certain distance before and after

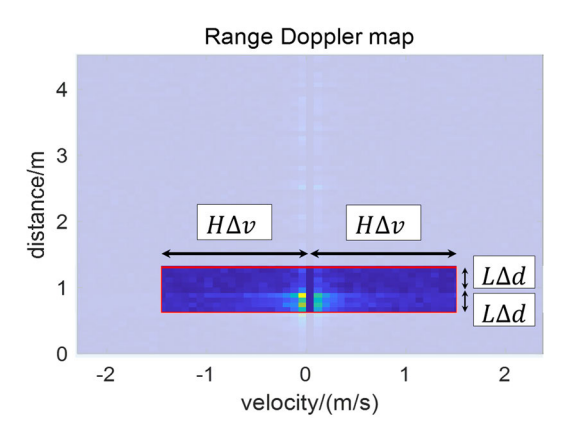


FIGURE 7. μ RDmap obtained via extraction. The figure illustrates the process of isolating the μ RDmap from the composite RD map. The highlighted red box indicates the specific range window around the target where critical motion information is concentrated.

the distance d_0 where the target is located, which is defined as the distance frames within the upper and lower edges of the red box. Moreover, v_h denotes the range within a certain velocity to the left and right of the 0-velocity frame as a red box.

B. MICRODOPPLER SIGNATURE FOR VELOCITY CLASSIFICATION

The first motion feature is the microDoppler signature, which represents the Doppler effect caused by the motion of the internal parts of the target:

$$MDS(v, n) = argmax_{|l| < L} |\mu RD(d_l(n), \theta_1, \theta_2, v, nT)|$$

$$(9)$$

where:

$$d_l = d_0(n) + l \times \Delta d$$
, and $|l| < L \in \mathbb{Z}$

As shown in Fig. 8, in this study, the method described in (9) yields the micro-Doppler signature from the μ RDmap. The waveform within each time frame is analyzed in Fig. 9, and the maximum intensity point corresponding to the target velocity is selected by

$$v(n) = \operatorname{argmax}_{v} \mathbf{MDS}(v, n) \tag{10}$$

C. HEIGHT SIGNATURE FOR HEIGHT CLASSIFICATION

The second motion feature, termed the height signature, was proposed to capture the height distribution of a target over time. The computation of the height signature involves the determination of the actual height of each point in the μRA_V map by considering the vertical arrival angle and the distance of the target from the radar. Moreover, the distribution of target heights within a given range can be obtained by leveraging the amplitude information of these points in the μRA_V map. Arranging these height distributions along the time axis provides insight into the height variation of the over time:

$$\mu RA_{V}(d, \theta_{2}, nT) = RA_{V}(d_{l}, \theta_{2}, nT)$$
(11)

where:

$$d = d_l = d_0(n) + l \times \Delta d$$
, and $|l| < L \in \mathbb{Z}$

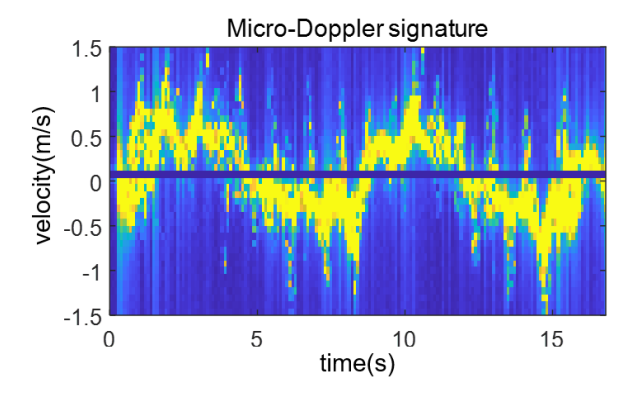


FIGURE 8. Micro-Doppler signature. This figure presents the micro-Doppler signature derived from the μ RDmap, capturing the velocity profile of the target. It shows the method used to select the peak intensity corresponding to the target's velocity.

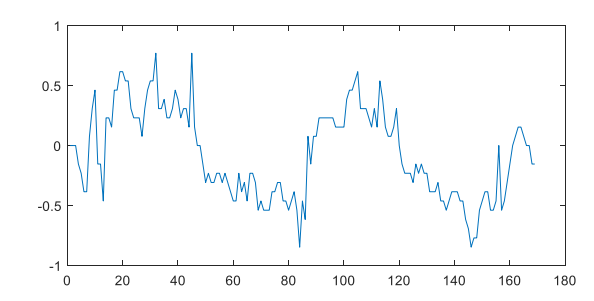


FIGURE 9. Velocity of the target. The process of extracting the target's velocity from the micro-Doppler signature is detailed.

The first step in calculating the height signature involves extracting the $\mu RA_V map$ calculated as described in (11) from the vertical component of the $RA_V map$, where L denotes the height range set relative to the radar:

$$h_q = d_l \cdot \sin(\theta_{2lq}) \tag{12}$$

$$\theta_{2lq} = \sin^{-1}\left(\frac{h_q}{d_l}\right) \tag{13}$$

where:

$$d_l = d_0(n) + l \times \Delta d$$
, and $|l| < L \in \mathbb{Z}$, $|q| < Q \in \mathbb{Z}$

Then, using the vertical angle of arrival and the distance associated with each point in the μRA_V map, the relative height of the target with respect to the radar can be calculated. This calculation involves determining the actual height corresponding to each point in the μRA_V map and thus provides an estimation of the vertical position of the target. These values are calculated as shown in (12) and (13).

Last, by considering the amplitude information associated with the points in the μRA_V map, the distribution of points within the height range of the target can be obtained. Furthermore, arranging these height distributions along the time axis



enables the examination of height variations in the target over time. The equation used for the calculation is as follows:

$$\textit{HS}(h_q, n) = \sum\nolimits_{l = -L}^{L} \textit{\muRA}_{V} \left(d, \theta_{2lq}, nT \right) \tag{14}$$

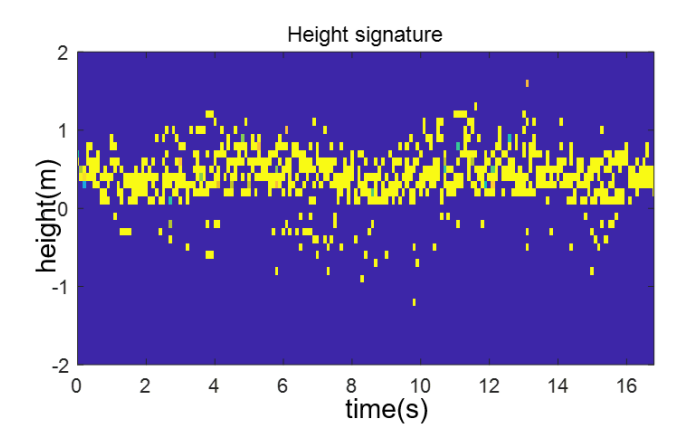


FIGURE 10. Height signature. This figure depicts the height signature calculated from the vertical radar data. It explains how the actual height of the target is computed using both the vertical angle and range information, which is then used to differentiate between high and low postures.

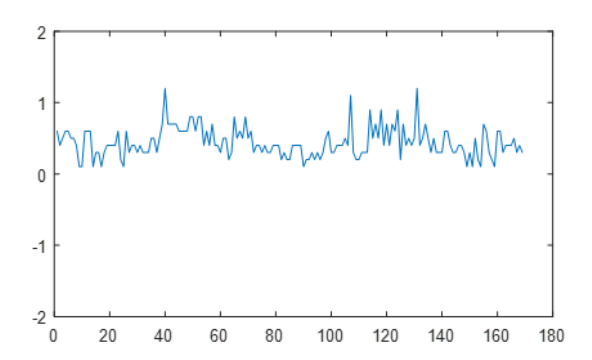


FIGURE 11. Height of target. Displayed here is the method for selecting the highest point in the height signature over time, which corresponds to the target's posture.

The results presented in Fig. 10 indicate that the height signature can be used as the height distribution of the target. Therefore, this section proposes a method by which to obtain the target height distribution based on selecting the highest point of the vertical axis in the height signature using the following equation. Figure 11 shows the results.

$$h(n) = argmax_{h_q} HS(h_q, n)$$
 (15)

D. POSITION CLASSIFICATION BASED ON FURNITURE RANGE

This part involved premeasuring the horizontal angle and distance ranges of the indoor furniture, relative to the radar. The target was allowed to move within a specified furniture range comprising doors, chairs, and beds. This furniture range was recorded with the radar in advance. Then, by utilizing the

range—angle map RA_H (d_0 , θ_1 , nT), the distance d_0 from the target to the radar and horizontal angle of arrival θ_1 are calculated. The temporal relationship between the target and the furniture was established by comparing the furniture range and target information, thus enabling the identification of whether the target is located near doors, beds, chairs, or open spaces.

E. MOTION STATE RECOGNITION METHOD VIA THRESHOLD COMPARISON

Micro-Doppler and height signatures were used for velocity and height classifications, respectively, which are explained later. The final section combines the results obtained from three classifications: velocity, height, and position. The method proposed in this section focuses on the motion features of the targets to recognize their motion states using the key features obtained from the three classifications.

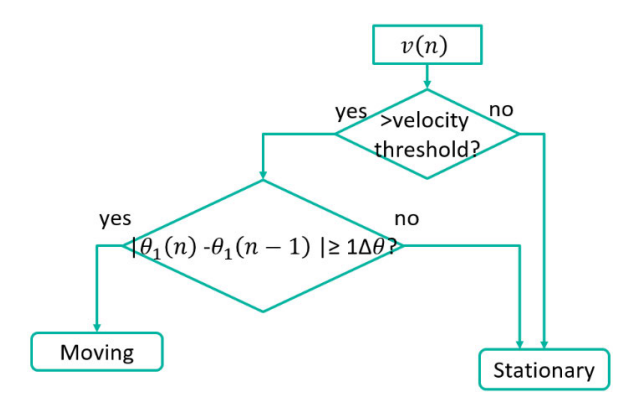


FIGURE 12. Flowchart of velocity classification. This flowchart outlines the steps involved in classifying the target's velocity. It includes details on threshold comparison and the integration of horizontal angle variation.

Firstly, the velocity is classified, and the velocity state of the target is obtained by comparing the v(n) obtained in (10) with the threshold value. The velocity threshold value in this study is Δv . The validation of the threshold value is presented in Section V-B. In addition, the relative velocity of the target is 0 when it is in tangential motion with respect to the radar. Hence, the change in the horizontal angle θ_1 is also incorporated into the comparison method. Figure 12 presents a flowchart of this method.

Next, the height is classified according to the h(n) obtained in (15) and compared with the threshold to obtain the height state of the target. The height threshold in this study is chosen as the chair height + target height \cdot 0.53, where 0.53 is the height ratio of the length of the chair surface to the top of the head when the target is seated to the height of the target [27]. Figure 13 presents a flowchart of this method.

The motion state recognition method proposed in this section integrates the three motion features of the target. The correlations between these features and the resulting motion states are illustrated in Table 1.

Because only the height-based binary categorization of high and low postures was designed in this study, sitting on

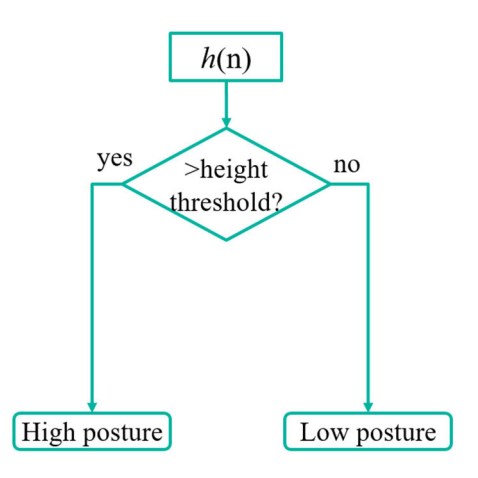


FIGURE 13. Height classification flowchart. This flowchart details the algorithm for height classification, from extracting the height signature to applying the height threshold. It emphasizes the rationale behind the selected threshold and the steps for categorizing high versus low postures.

the bed was considered as lying on the bed. By combining the results obtained using appropriate labels, the motion state of the target can be recognized. Figure 14 presents a comprehensive summary flowchart of motion state recognition.

This study uses a 60GHz FMCW radar to first extract the RDmap of the target, generate micro-Doppler features and altitude features, and then identify the human body's movement state through threshold classification of velocity, altitude, and position information. In addition, to address the concern of oversimplification, this study provides a detailed and reasonable analysis of the threshold selection and verifies its effectiveness in various real-world scenarios through experiments.

TABLE 1. Classification correlation.

Loation Velocity & Height	Open space	Door	Chair	Bed
Moving High posture	Walking	Coming in /out	Walking	Walking
Stationary High posture	Standing	Standing	Standing	Standing
Moving Low posture				
Stationary Low posture			Sitting	Lying

This table summarizes the relationships between velocity, height, and position features and their corresponding motion states, forming the basis for threshold-based motion recognition.

V. RESULTS

A. RADAR SPECIFICATIONS

The radar specification parameters are listed in Table 2. The radar used in this study was an Infineon BGT60TR13c

TABLE 2. Radar parameters.

This table lists the technical specifications of the FMCW radar used in the study, including frequency, bandwidth, antenna configuration, and resolution, which are critical for motion detection.

Parameter Name	Value
Carrier frequency	60.5GHz
Frequency bandwidth	2GHz
Sampling interval	1 µsec
Number of samplings per chirp	128
Number of chirps per frame	64
Frame Frequency	10Hz
Max Distance	4.736m
Distance resolution	0.074m
Max velocity	2.45m/s
Velocity resolution	0.077m/s
Height above the ground	1.2m

FMCW radar. The 60 GHz radar has one transmitting antenna (Tx) and three receiving antennas (Rx0, Rx1, and Rx2). Among them, the horizontal angle of arrival can be measured by the received signal of Rx0 and Rx1, and the vertical angle of arrival can be measured by the received signal of Rx0 and Rx2. Moreover, the spacing between the antennas is $\frac{\lambda}{2}$.

B. THRESHOLD LEVEL FOR VELOCITY CLASSIFICATION

To evaluate the accuracy of the velocity measurement and classification using a threshold comparison, we devised eight scenarios involving different types of indoor movements.

Case #1: An empty chair without an object was placed directly in front of the radar.

Case #2: There is a stationary target in the chair; for example, a person sleeping, and there is no movement in the seat

Case #3: The target moves slightly in the chair; for example, a person who is reading a book and moves his/her head with his/her hands.

Case #4: The target stands still in front of a chair; for example, a person who is standing and thinking with almost no movement.

Case #5: The target stands with slight movement in front of a chair; for example a person standing and using a cell phone with slight head and hand movements.

Case #6: The target walks in front of the radar.

Case 7: There is a fan on the chair directly in front of the radar, and the fan is powered off and stationary. There are no human targets in the rooms.

Case #8: The fan on the chair directly in front of the radar is continuously powered during cut running. There are no human targets in the rooms.

Figure 15 depicts the Doppler spectrum of the selected vital sign features extracted from a certain timeframe within the



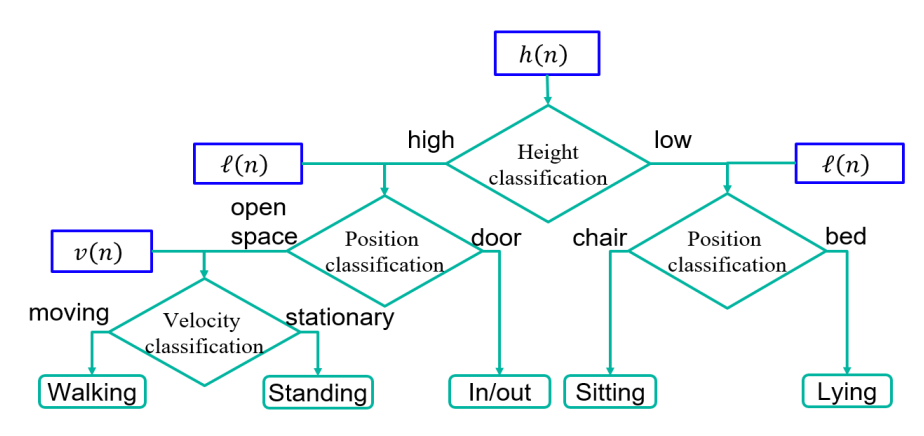


FIGURE 14. Flowchart of motion recognition. This comprehensive flowchart integrates the velocity, height, and position classification processes. It visually summarizes the complete motion recognition methodology, showing how individual feature analyses are combined to determine the overall motion state.

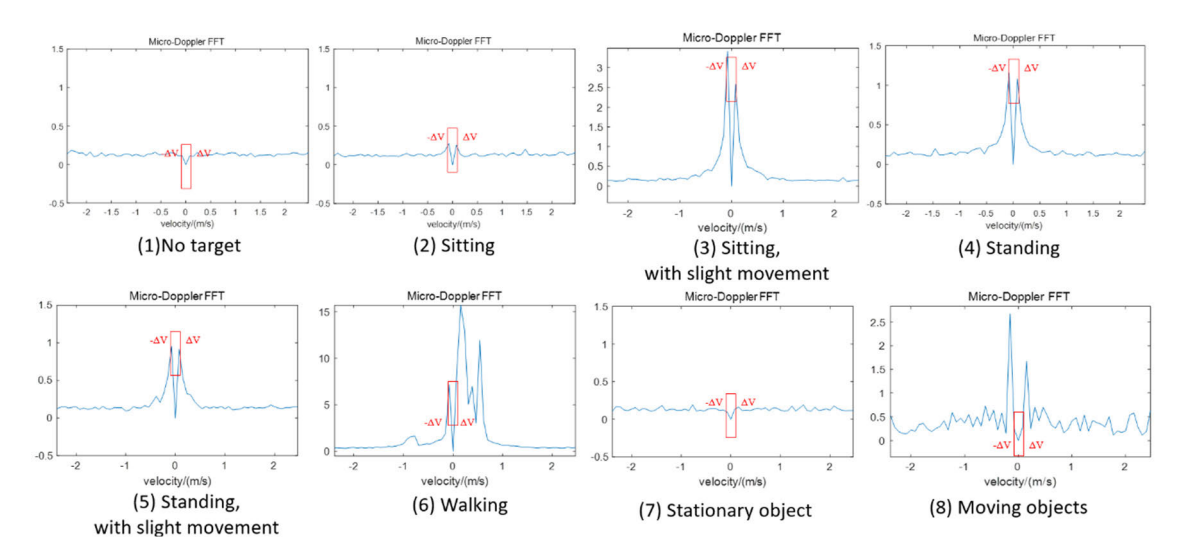


FIGURE 15. Velocity measurement scenarios (zero Dopplers are forced to an amplitude of zero). This figure illustrates the velocity feature values of various targets, including stationary objects, moving objects, and human in different postures. The red-dotted boxes highlight the velocity range within $\pm \Delta v$, which serves as the velocity threshold for classification. These visualizations provide an intuitive understanding of how different motion states—such as sitting, standing, walking, and non-human object motion—correlate with the velocity threshold, aiding in accurate motion state recognition.

micro-Doppler signature. The velocity (m/s) is represented on the x-axis and the amplitude is indicated on the y-axis. Furthermore, the red-dotted boxes highlight the velocity region of the target within the range of $\pm \Delta v$.

Three features were extracted from these micro-Doppler images. The first is whether a velocity peak exists, from which we can determine whether a target is present.

The second is whether the velocity peak is on or off the boundary of $\pm \Delta v$, from which we can determine whether the target or object is moving or relatively stationary.

The third factor is the number of velocity peaks and whether they are coherently distributed, from which we can determine whether they come from human targets or objects.

Therefore, we decided to set the velocity threshold of velocity classification as Δv .

C. THRESHOLD LEVEL FOR HEIGHT CLASSIFICATION

To validate the proposed height classification scheme for the target, we conducted measurement scenarios involving radar placement at six different heights. The target actions in each scenario were recorded, which involved continuous sitting for 10 s that was followed by standing for 10 s and lying on the ground for 10 s.

Figure 16 shows the height signature of the radar signal after processing the reflected wave generated by the movement of the target at the six aforementioned altitudes.

Recalling (12), the height h is related to the sine function, and the change in sine or h is most sensitive when the vertical angle is approximately 0. In this study, the height of the target when sitting is generally 1.2 to 1.3 m. Therefore, when the radar is placed at 1.2 m, the height distribution of several

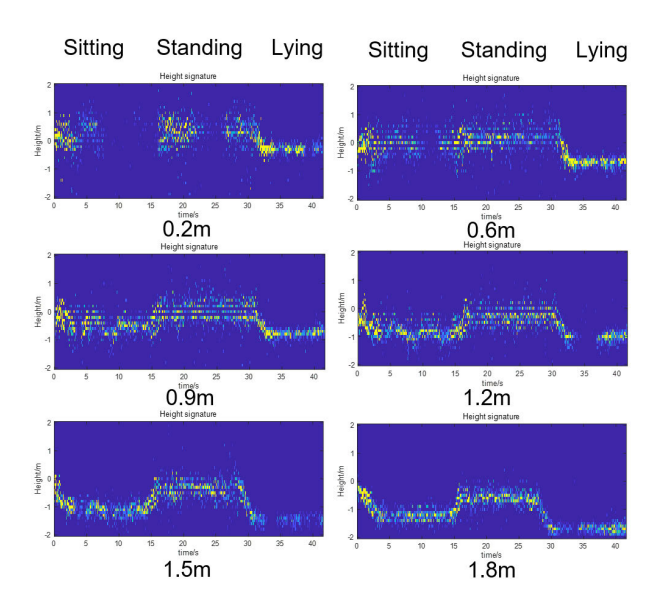


FIGURE 16. Height signatures when the radar is at different heights. This figure compares the height signatures obtained from the radar when mounted at various heights. It demonstrates how radar placement affects the height distribution and provides insights into selecting the optimal mounting height for accurate posture detection.

actions is different, compared with other heights. Hence, we can perform height classification.

D. DESIGN AND ENVIRONMENT

An important aspect of the performance of our method is its adaptability to different targets. To validate the proposed method, we recognized the motion states by employing a threshold comparison method. In this section, we describe the experimental environment and layout.

The experiment scenario is mainly assumed to be at night or unattended, with a single person living alone or in a

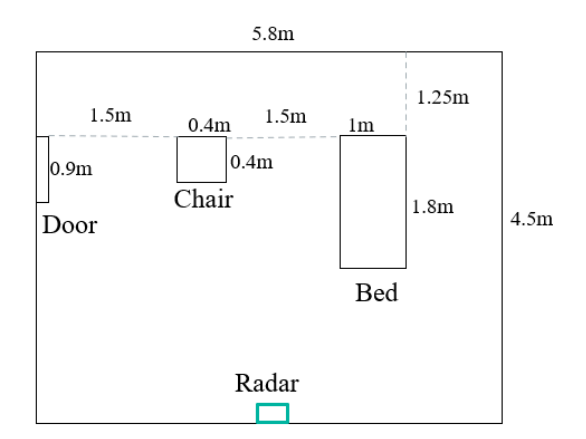


FIGURE 17. Graph of the experimental environment. This diagram offers a detailed layout of the experimental environment, including the dimensions of the room and the placement of major furniture. It helps clarify the spatial relationships between the radar, targets, and obstacles during the experiments.

private room in a facility. The main pieces of furniture in the environment, from left to right, are a door, chair, and bed. We measured the dimensions of the rooms within the experimental environment as well as the furniture placement. The obtained measurements are arranged in a planar graph, as illustrated in Fig.17.

Table 3 lists the targets of these experiments. Each individual was moved to a room. These data were used in the proposed method to recognize the motion state results. The results were compared using video recorded by the camera to assess accuracy.

In the experiment, different movements were individually recorded for each target in the room, each of which lasted for approximately 30 s. The movements included sitting, lying down, standing, and walking.

TABLE 3. Target's data.

Gender	Height(cm)
Female	164
Female	169
Male	179
Male	169
Female	163
Male	173
Male	167
Male	170
Male	175
Male	181

This table presents the demographic and physical characteristics of the participants in the experiments, ensuring diversity in evaluating the proposed method.

E. EXPERIMENTAL RESULTS AND EVALUATION OF MOTION STATE RECOGNITION

To evaluate the effectiveness of the proposed threshold comparison method in determining the motion states of an indoor target, we used a traditional support vector machine (SVM) method for these motion state data to make a comparison.

TABLE 4. SVM accuracy.

1	2	3	4	5	6
65.80%	66.26%	64.31%	65.30%	66.10%	64.74%
7	8	9	10	mean	cost time
65.42%	64.72%	62.84%	64.33%	64.98%	32 hours

This table shows the motion recognition accuracy of a traditional support vector machine (SVM) method, serving as a benchmark for comparison with the proposed threshold-based approach.



In the traditional SVM method, the data consist of RD maps of 40 sets of motion data regarding 10 targets from 3 receiving antennas. Each 64×64 RD map is regrouped into 1×4096 vectors and input into the SVM, using RBF as the kernel function. Cross-validation is performed using the K-fold method, where K=10. Table 4 presents the accuracy of the results of the 10 validations along with their average values.

TABLE 5. Threshold comparison accuracy.

Target	Sitting	Lying	Standing	Walking	Mean
Female 164cm	86.5%	87.3%	80.6%	80.4%	83.7%
Female 169cm	97.9%	89.7%	95.7%	93.3%	94.15%
Male 179cm	95.4%	96.7%	97.1%	96.6%	96.45%
Male 169cm	83.8%	52.5%	78.5%	73.4%	72.05%
Female 163cm	97.4%	87.7%	96.7%	63.1%	86.23%
Male 173cm	75.8%	98.6%	100%	75.9%	87.58%
Male 167cm	89.7%	66.6%	97.0%	67.3%	80.15%
Male 170cm	94%	98.1%	100%	70%	90.53%
Male 175cm	75.1%	89%	98.9%	70%	83.25%
Male 181cm	61.3%	94.4%	90.7%	71.7%	79.53%
Mean	85.7%	86.1%	93.5%	76.2%	85.4%

This table provides the recognition accuracy of the proposed threshold comparison method across different motion states, demonstrating its effectiveness and reliability in indoor monitoring.

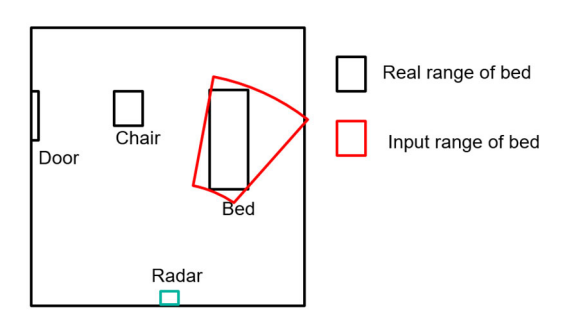


FIGURE 18. Graph of the range of the bed. This figure zooms in on the range data for the bed, as captured by the radar. It explains the impact of the RAmap's polar coordinate system on accurately determining the furniture range and discusses potential misclassification issues arising from this representation.

Table 5 shows the accuracy and mean of the recognition results for the 10 targets whose data were recognized by the proposed threshold comparison method. The total time required to recognize the motions of the 10 targets was approximately 3 min. The average accuracy of the four motions was 85.4%. The average accuracies for sitting on a chair, lying on a bed, standing, and walking were 85.7%,

93.5%, and 76.2%, respectively. Combining these results with those shown in Table 1, standing and walking rely on velocity classification for separation. Moreover, these results can be affected by the limb movement caused by individual differences in the target while standing.

In addition, as shown in Fig.18, we found that because the radar RAmap uses a polar coordinate system, the input furniture range will usually behave as a circular sector that is much larger than the real furniture range in specific cases, which leads to the walking movement being misrecognized as a lying motion. Therefore, we propose the following for future research: (1) Improve the calculation accuracy of the angle of arrival, which means improving the resolution of the horizontal angle. (2) Convert the RDmap polar coordinate system into a rectangular coordinate system. (3) Use at least two radars to construct the signal receiving system.

This study also validated the performance of the feature extraction-SVM hybrid algorithm. In this experiment, the input features for the SVM are not RDmap, but rather the distance, velocity, height, and polar coordinates of the target extracted from the RDmap. This algorithm achieves extremely high accuracy. Compared to the original SVM algorithm, the higher accuracy and faster training speed demonstrate the accuracy of the feature extraction proposed in this study. The performance results of the original SVM, feature extraction-SVM, and feature extraction-threshold comparison algorithms are shown in Table 6.

TABLE 6. Performance results of three algorithms.

	Mean Accuracy
Origin SVM	64.98%
Feature extraction- SVM	91.26%
Feature extraction- threshold comparison	85.40%

This table shows the action recognition accuracy of the original SVM, feature extraction-SVM, and feature extraction-threshold comparison algorithms.

This experiment assumes that in a new experimental setting with a new environmental layout, we will explore new classification methods. The input data for the three algorithms is the same, and the types of motion states recognized in the results are also the same. The experiment results show that:

1) ORIGINAL SVM

The algorithm is simple, but it has low accuracy, long training time, and requires training data.

2) FEATURE EXTRACTION-SVM

It has a shorter training time and high accuracy, but the classification boundary is difficult to explain physically

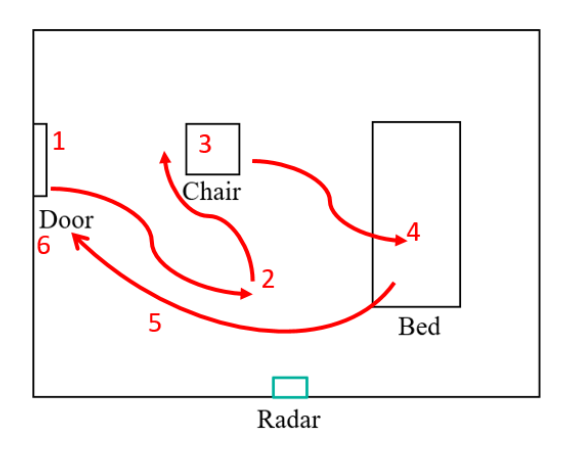


FIGURE 19. Furniture range map and target motion sequence. The motion sequence of the experiment target is: open the door and enter the room, walk to the front of the radar and stand for 10 seconds, walk to the chair and sit down for 10 seconds, get up and walk to the bed and lie down for 10 seconds, get up and walk to the door, open the door and walk out of the room.

and requires training data. When the environmental layout changes, new training data is needed.

3) FEATURE EXTRACTION-THRESHOLD COMPARISON

High accuracy, easy-to-understand and adjustable thresholds, no training data required, quick adaptation to changes in target and environment layout, but requires pre-input of target height and furniture range.

F. EVALUATION OF CONTINUOUS MOTION STATE RECOGNITION

In single room with different furniture layouts, 3 additional targets conducted continuous motion recognition experiments. As shown in Figure 19, the sequence of motions for the experiment target is as follows:

Open the door and enter the room.

Walk to the front of the radar and stand there for 10 seconds.

Walk to the chair and sit down for 10 seconds.

Get up, walk to the bed, and lie down for 10 seconds.

TABLE 7. Recognition results of continuous motion.

Accuracy
90.0%
90.3%
91.3%

This table shows the performance of the threshold comparison algorithm in terms of continuous motion recognition accuracy for three experiment targets with different genders and heights.

Get up, walk to the door, open the door, and exit the room. As shown in Table 7, the experiment resulted in a continuous motion recognition accuracy rate of over 90%.

The results show that the motion state recognition method using the FMCW radar for a threshold comparison of velocity, height, and position is feasible in the field of indoor monitoring. Moreover, the threshold comparison method is superior to the traditional SVM method in terms of accuracy, cost, time, and ease of understanding the motion features.

VI. CONCLUSION

The objective of this study was to develop a system that can monitor targets in daily indoor activities using FMCW radar. We propose a method based on velocity, height, and position classifications to recognize the motion state of an indoor single target via threshold comparison. In addition, we performed three main experiments on: the velocity threshold for velocity classification, the radar height for height classification, and the 4 motion states of 10 targets in the room.

In the first experiment, the RD map, MD signature, and other images of the target in various scenes were compared, and the appropriate velocity threshold was determined. In the second experiment, the setting height of the radar was determined by comparing the height signatures of the radar set at each height. In addition, experiments on single and continuous movements were conducted using the motion state recognition method for different heights and sexes, and the results showed that the average accuracy of the motion state recognition exceeded 85%.

Compared with the machine learning method typically used for motion state recognition, the proposed method for monitoring the motion states of indoor targets using FMCW radar offers a new method with several distinct advantages. The key differentiating factor is the exclusive use of the threshold comparison method. This feature simplified the calculation process and improved the generalizability of the results. In addition, for the feature extraction method in the MD and height signatures of the proposed method, we found that even if it is not applied to the threshold comparison method, it has the potential to improve processing time and increase accuracy, even when used with other motion recognition methods.

By utilizing a threshold comparison, the proposed method eliminates the need for complex machine learning models and large training datasets. This simplification reduces computational complexity and resource requirements, making the method more convenient and efficient in practice. Moreover, the proposed method is expected to be implemented on smaller processing units, which is more relevant to the application scenario of this study, such as monitoring and watching over the elderly or patients during their daily indoor activities. Furthermore, it is easier to perform motion state recognition because machine learning is not required. The thresholds used in the proposed method can be customized to pre-determined values based on the indoor environment



and application requirements, resulting in a transparent and intuitive calculation process. This adaptability and generalizability allowed us to obtain reliable performances in different environments without the need for extensive training data.

Despite the promising results demonstrated in this study, several limitations should be noted:

In addition, this study also conducted tests in complex environments to explore the limits of the proposed method. In the test scenario, which included target occlusion and environmental noise (such as fans and air conditioners), it was difficult to identify the distance frame of the target in RDmap, leading to failures in target position calculation and target feature extraction, leading to potentially affecting classification accuracy.

The current method relies on the pre-input of the target's height and is primarily designed for single-target monitoring. In multi-target scenarios, when multiple targets maintain a certain distance, the system can accurately identify each target (approximately 4 to 5 targets at a maximum distance of 4.5m). However, since the proposed method relies on pre-input target height, under the current algorithm, it is unable to track multiple targets and their corresponding heights, leading to target confusion, which leads to target confusion and reduces the robustness of motion state recognition.

The threshold-based classification method, while efficient and interpretable, may be sensitive to overlapping motions, complex activities, and diverse motion patterns that were not extensively investigated in this work. This limits the immediate applicability of the method in more complex real-world environments.

In the future, to further improve the accuracy of the motion state, the method should improve the error reduction of the final result and reduce the confusion between different motions. To address these limitations, future work will focus on enhancing the robustness of the system through improved noise reduction techniques and advanced signal processing algorithms. Additionally, the classification method used for several types of motion features must be adaptable to more complex application scenarios, such as falls and heart rate respiration detection.

REFERENCES

- T. Huang, G. Liu, S. Li, and J. Liu, "RPCRS: Human activity recognition using millimeter wave radar," in *Proc. IEEE 28th Int. Conf. Parallel Distrib. Syst. (ICPADS)*, Jan. 2023, pp. 122–129.
- [2] H. Cui and N. Dahnoun, "High precision human detection and tracking using millimeter-wave radars," *IEEE Aerosp. Electron. Syst. Mag.*, vol. 36, no. 1, pp. 22–32, Jan. 2021.
- [3] G. Wang, C. Gu, T. Inoue, and C. Li, "A hybrid FMCW-interferometry radar for indoor precise positioning and versatile life activity monitoring," *IEEE Trans. Microw. Theory Techn.*, vol. 62, no. 11, pp. 2812–2822, Nov. 2014.
- [4] B. Liu, M. Jian, Z. Lu, and R. Chen, "Indoor monitoring human movements using dual-receiver radar," in *Proc. IEEE Radar Conf. (RadarConf)*, May 2017, pp. 0520–0523.
- [5] G. Zhang, X. Geng, and Y.-J. Lin, "Comprehensive mPoint: A method for 3D point cloud generation of human bodies utilizing FMCW MIMO mmwave radar," Sensors, vol. 21, no. 19, p. 6455, Sep. 2021.

- [6] D. Xu, Y. Liu, and Q. Wang, "Random forest-based human pose detection system for through-the-wall radar," *J. Phys., Conf. Ser.*, vol. 1966, no. 1, Jul. 2021, Art. no. 012040.
- [7] L. J. Dirksmeyer, A. Marnach, D. Schmiech, and A. R. Diewald, "Developing of algorithms monitoring heartbeat and respiration rate of a seated person with an FMCW radar," *Adv. Radio Sci.*, vol. 19, pp. 195–206, Dec. 2021.
- [8] H.-I. Choi, W.-J. Song, H. Song, and H.-C. Shin, "Improved heartbeat detection by exploiting temporal phase coherency in FMCW radar," *IEEE Access*, vol. 9, pp. 163654–163664, 2021.
- [9] Y.-K. Yoo, C.-W. Jung, and H.-C. Shin, "Unsupervised detection of multiple sleep stages using a single FMCW radar," *Appl. Sci.*, vol. 13, no. 7, p. 4468, Mar. 2023.
- [10] Y. Chen, Y. Luo, J. Ma, A. Qi, R. Huang, F. De Paulis, and Y. Qi, "Non-contact in-vehicle occupant monitoring system based on point clouds from FMCW radar," *Technologies*, vol. 11, no. 2, p. 39, Mar. 2023.
- [11] T. Gänzle, C. Klöck, and K. Heuschkel, "Real-time vital sign detection using a 77 GHz FMCW radar," in *Proc. IEEE-EMBS Conf. Biomed. Eng. Sci. (IECBES)*, Dec. 2022, pp. 148–153.
- [12] Y. Kim and H. Ling, "Human activity classification based on micro-Doppler signatures using a support vector machine," *IEEE Trans. Geosci. Remote Sens.*, vol. 47, no. 5, pp. 1328–1337, May 2009.
- [13] M. S. Seyfioglu, A. M. Özbayoglu, and S. Z. Gürbüz, "Deep convolutional autoencoder for radar-based classification of similar aided and unaided human activities," *IEEE Trans. Aerosp. Electron. Syst.*, vol. 54, no. 4, pp. 1709–1723, Aug. 2018.
- [14] Y. Kim and T. Moon, "Human detection and activity classification based on micro-Doppler signatures using deep convolutional neural networks," *IEEE Geosci. Remote Sens. Lett.*, vol. 13, no. 1, pp. 8–12, Jan. 2016.
- [15] M. S. Seyfioglu, B. Erol, S. Z. Gurbuz, and M. G. Amin, "DNN transfer learning from diversified micro-Doppler for motion classification," *IEEE Trans. Aerosp. Electron. Syst.*, vol. 55, no. 5, pp. 2164–2180, Oct. 2019.
- [16] S. Hochreiter and J. Schmidhuber, "Long short-term memory," Neural Comput., vol. 9, no. 8, pp. 1735–1780, Nov. 1997.
- [17] G. Klarenbeek, R. I. A. Harmanny, and L. Cifola, "Multi-target human gait classification using LSTM recurrent neural networks applied to micro-Doppler," in *Proc. Eur. Radar Conf. (EURAD)*, Oct. 2017, pp. 167–170.
- [18] M. Wang, G. Cui, X. Yang, and L. Kong, "Human body and limb motion recognition via stacked gated recurrent units network," *IET Radar, Sonar Navigat.*, vol. 12, no. 9, pp. 1046–1051, Sep. 2018.
- [19] F. Shamsfakhr, M. Corrà, A. Ferrari, D. Macii, L. Palopoli, and D. Fontanelli, "Algorithms for enhanced indoor positioning and tracking based on a 60-GHz radar platform," in *Proc. IEEE Int. Workshop Metrol*ogy Ind., Jun. 2022, pp. 184–189.
- [20] S. P. Rana, M. Dey, H. U. Siddiqui, G. Tiberi, M. Ghavami, and S. Dudley, "UWB localization employing supervised learning method," in *Proc. IEEE 17th Int. Conf. Ubiquitous Wireless Broadband (ICUWB)*, Sep. 2017, pp. 1–5.
- [21] S. P. Rana, M. Dey, R. Brown, H. U. Siddiqui, and S. Dudley, "Remote vital sign recognition through machine learning augmented UWB," in *Proc.* 12th Eur. Conf. Antennas Propag. (EuCAP), Apr. 2018, pp. 5–619.
- [22] M. Jia, S. Li, J. L. Kernec, S. Yang, F. Fioranelli, and O. Romain, "Human activity classification with radar signal processing and machine learning," in *Proc. Int. Conf. U.K.-China Emerg. Technol. (UCET)*, Aug. 2020, pp. 1–5, doi: 10.1109/UCET51115.2020.9205461.
- [23] J. Zabalza, C. Clemente, G. Di Caterina, J. Ren, J. J. Soraghan, and S. Marshall, "Robust PCA micro-Doppler classification using SVM on embedded systems," *IEEE Trans. Aerosp. Electron. Syst.*, vol. 50, no. 3, pp. 2304–2310, Jul. 2014, doi: 10.1109/TAES.2014.130082.
- [24] A. Lazaro, M. Lazaro, R. Villarino, and D. Girbau, "Seat-occupancy detection system and breathing rate monitoring based on a low-cost mmwave radar at 60 GHz," *IEEE Access*, vol. 9, pp. 115403–115414, 2021.
- [25] L. Zhao, M. Yangyang, Z. Yang, L. Fulai, Y. Xiao, Q. Fugui, L. Hao, L. Guohua, and W. Jianqi, "UWB radar features for distinguishing humans from animals in an actual post-disaster trapped scenario," *IEEE Access*, vol. 9, pp. 154347–154354, 2021.
- [26] H. Xue, Y. Ma, Y. Zhang, Z. Zhang, G. Shi, J. Wang, and H. Lv, "Distinction of human and mechanical vibrations within similar frequency bands based on wavelet entropy using ultrawideband radar," *Appl. Sci.*, vol. 12, no. 19, p. 10046, Oct. 2022.
- [27] P. Chandna, S. Deswal, and A. Chandra, "An anthropometric survey of industrial workers of the northern region of India," *Int. J. Ind. Syst. Eng.*, vol. 6, no. 1, pp. 110–128, 2010.





RUOYU HE received the B.S. degree in engineering from Nanjing University of Aeronautics and Astronautics, China, in 2019, and the M.S. degree in engineering from The University of Electro-Communications, Tokyo, Japan, in 2023, where he is currently pursuing the Ph.D. degree in engineering. His research interests include biomedical engineering, non-contact sensors, vital sign detection, and signal processing.



MASAKI KUROSAWA received the B.E. and M.E. degrees in electronics and communication engineering from Waseda University, Tokyo, Japan, in 1979 and 1981, respectively, and the Ph.D. degree in electrical engineering from the University of Tennessee, Knoxville, TN, USA, in 1991. He is currently a Visiting Researcher with The University of Electro-Communications, Tokyo, Japan. He is a member of the Institute of Electronic, Information and communication Engineers (IEICE), Tokyo.



GUANGHAO SUN (Senior Member, IEEE) received the B.S. degree in medical engineering from Chiba University, Chiba, Japan, in 2011, and the M.S. and Ph.D. degrees in system design engineering from Tokyo Metropolitan University, Tokyo, Japan, in 2013 and 2015, respectively. He completed the Frontier Science Course supported by the Ministry of Education, Culture, Sports, Science and Technology (MEXT), Japan, in 2011. From April 2013 to September 2015,

he was a Research Fellow with Japan Society for the Promotion of Science. In 2015, he was with The University of Electro-Communications, Tokyo, Japan, as an Assistant Professor, where he became an Associate Professor, in 2020. His research interests include non-contact bio-measurement, bio-signal processing, and design medical instrumentation. He is a Senior Member of IEEE Engineering in Medicine and Biology Society (IEEE-EMBS) and Japanese Society for Medical and Biological Engineering (JSMBE). He was a recipient of the 2013 BES-SEC Design Silver Award for design a multiple vital-signs based infection screening system and the 2014 Chinese Government Award for Outstanding Self-financed Student

. . .